CAV2021
11th International Symposium on Cavitation
May 10-13, 2021, Daejon, Korea

Nuclei transport about a sphere

Rhys A. Paul[1]*, James A. Venning[1] and Paul A. Brandner[1]

[1]Cavitation Research Laboratory, University of Tasmania, Launceston, Tasmania, Australia

Abstract: Microbubble transport in a potential flow about a sphere is studied. A system of differential equations is solved numerically to model the propagation of microbubbles subject to the Kelvin impulse, pressure gradients and drag. Buoyancy due to the pressure gradient is found to be the dominant force, but the deviation from streamlines is small. Finally, the inclusion of a viscous boundary layer is shown to prevent bubbles colliding with the sphere surface.

Keywords: Microbubbles; Screening; Activation; Potential Flow

1. Introduction

A microbubble advected by a potential flow will deviate from the streamlines due to complex forces which occur as a one-way interaction by the flow on the microbubble. While the pressure field produced by an inviscid potential flow around a sphere reaches a minimum pressure at the maximum ordinate, predicting the trajectory and pressure history of an advected microbubble is not straight-forward. Johnson and Hsieh [1] have shown that some bubbles advected around a blunt body may be 'screened' by the region of high pressure near the stagnation point and are prevented from reaching the low-pressure region. Brandner et al [2] have found that the rate of cavitation events predicted by potential flow around a sphere are an order of magnitude greater than is seen in experiments. Similar conclusions result from the analytical model investigated by Liu et al [3].

In this paper, the forces acting on a microbubble are modelled during advection past a sphere. The fluid moves according to a classical potential flow, with a laminar boundary layer near the sphere's surface. The bubble motion is governed by a force acting as applied to Newton's second law and its growth according to the Rayleigh-Plesset equation. The relative effect of each force is considered for a typical trajectory, and the effect of the pressure gradient is shown to dominate other forces. Finally, the inclusion of a viscous boundary layer is shown to prevent bubbles from colliding with the sphere's surface.

2. Numerical model

A sphere of radius a is considered in a fluid flowing with freestream speed u_∞. A Cartesian coordinate system is located with the origin at the centre of the sphere. The positive z-axis is oriented to point in the direction of the freestream fluid motion and y-axis pointing upwards. Due to the symmetry of the model, it is often useful to use both Cartesian and spherical coordinate systems. As such, the polar angle θ is measured clockwise from the forward stagnation point and distance r from the sphere's centre. A schematic of the system is given in Figure 1. All results presented here are computed with $a = 75$ mm.

The components of the fluid velocity $\boldsymbol{u} = u_r\hat{e}_r + u_\theta\hat{e}_\theta$ follow from classical inviscid theory

$$u_r = -u_\infty\left[1 - \left(\frac{a}{r}\right)^3\right]\cos(\theta); \quad u_\theta = u_\infty\left[1 + \frac{1}{2}\left(\frac{a}{r}\right)^3\right]\sin(\theta) \tag{1}$$

and the corresponding pressure field is given by Bernoulli's principle.

The characteristic flow parameters are the cavitation number σ and sphere Reynolds number Re_s, defined to be

* Corresponding Author: Rhys A. Paul, Rhys.Paul@utas.edu.au

$$\sigma = \frac{P_0 - P_v}{\frac{1}{2}\rho u_\infty}; \quad Re_s = \frac{2au_\infty}{\nu} \tag{2}$$

Here P_0 is the freestream static pressure measured at the height of the forward stagnation point, P_v is vapor pressure, ρ is the density of the fluid and ν is the kinematic viscosity.

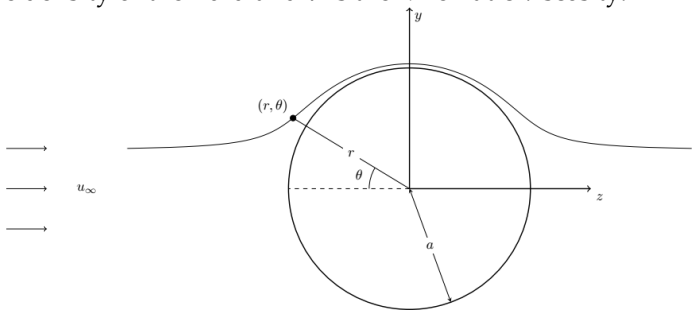

Figure 1. A schematic of the coordinate system orientation and example streamline about the sphere.

The bubbles are assumed to remain spherical and the Rayleigh-Plesset equation is used to model the change in radius R (Franc and Michel [4](P.37):

$$\rho\left[R\frac{d^2R}{dt^2} + \frac{3}{2}\left(\frac{dR}{dt}\right)^2 + \frac{4\nu}{R}\frac{dR}{dt}\right] = P_v + P_{g0}\left(\frac{R_0}{R}\right)^{3k} - P - \frac{2\gamma}{R} \tag{3}$$

where P_{g0} is the pressure inside the bubble at equilibrium, R_0 is the initial bubble radius, k is the polytropic index, P is the pressure of the fluid at the location of the bubble and γ is the surface tension parameter.

Following the derivation presented by Johnson and Hsieh [1], the equation of motion describing the trajectory of the bubble follows from a consideration of the component forces. Some minor simplification yields a differential equation for the bubble velocity $\boldsymbol{w}$:

$$\frac{2}{3}\pi\rho R^3\frac{d\boldsymbol{w}}{dt} = 2\pi\rho R^2(\boldsymbol{u}-\boldsymbol{w}) + \frac{1}{2}\pi\rho C_D R^2(\boldsymbol{u}-\boldsymbol{w})|\boldsymbol{u}-\boldsymbol{w}| - 2\pi R^3\boldsymbol{\nabla}P \tag{4}$$

The drag coefficient C_D is calculated from an empirical equation [1]:

$$C_D = \frac{24}{Re_b}\left(1 + 0.197{Re_b}^{0.63} + 2.6\times10^{-4}{Re_b}^{1.38}\right) \tag{5}$$

wherein Re_b is the Reynolds number of the bubble, defined to be

$$Re_b = \frac{2R|\boldsymbol{u}-\boldsymbol{w}|}{\nu}. \tag{6}$$

The first term on the right side of equation 4 is due to the Kelvin impulse, the second term accounts for the drag due to velocity difference between the bubble and carrier fluid, and the final term represents the force due to pressure gradients.

Equations 3 and 4 are integrated using a stiff Runge-Kutta integrator until the microbubble reaches the meridian at $\theta = \pm\pi/2$, Collides with the surface of the sphere, or reaches critical pressure.

Bubbles are assumed to activate if they experience a local fluid pressure lower than the Blake critical pressure, *Pc*. An expression for the Blake critical pressure is given by Brennen [5](p.52):

$$P_c = P_v - \frac{4\gamma}{3R_0}\sqrt{\frac{2\gamma}{3kR_0P_{g0}}}. \tag{7}$$

Figure 2 compares typical trajectories of microbubbles (solid lines) and corresponding streamlines (dashed lines), for varying initial bubble heights y_0. The initial bubble radius, cavitation number and Reynolds numbers are all held constant, with $R_0 = 50\ \mu$m, $\sigma =$ 0.8 and $Re_s = 10^6$. Three of the four bubbles experience pressures below P_c (black dashed line) and are activated. The trajectories do not

* Corresponding Author: Rhys A. Paul, Rhys.Paul@utas.edu.au

deviate noticeably from the streamline until they near the sphere, where the local pressure gradient pushes the bubbles away from the leading stagnation point. Near the top of the sphere, the direction of the pressure gradient inverts, and the bubbles are drawn inwards.

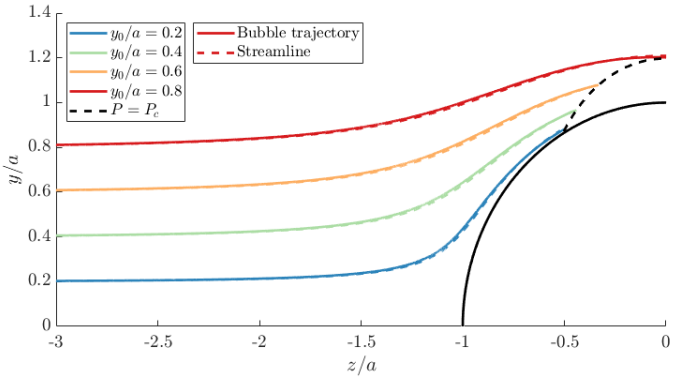

Figure 2. Typical trajectories of microbubbles compared with streamlines passing through the same starting conditions, for $R_0 = 50\ \mu$m, $\sigma = 0.8$ and $Re_s = 10^6$. The solid black line denotes the edge of the sphere and dashed black line the critical pressure contour.

The individual force components acting on the bubble starting at $y_0 = a$ (red line) are presented in Figure 3 and are broken into components tangential (a) and transverse (b) to the motion of the bubble. In each case the effects of the Kelvin impulse and drag are small compared to pressure gradients, particularly as the bubble nears the top of the sphere where the strong negative gradient draws it towards the surface. Even for a large bubble there is very little deviation from the streamline and the overall screening effect is small. This is consistent with the findings of Liu et al [3], who noted that screening effects on a sphere were insufficient to explain discrepancies in the cavitation event rate predicted analytically with that observed experimentally.

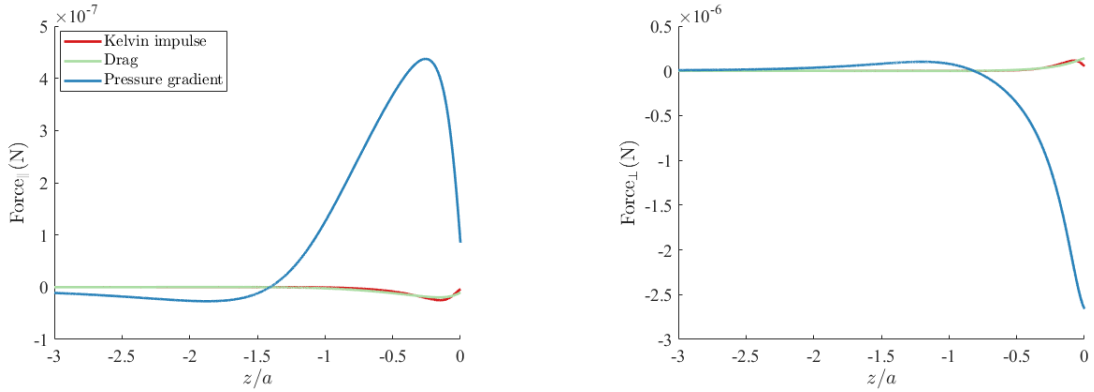

Figure 3. Force components acting tangential (a) and transverse (b) to the velocity of a microbubble with $R_0 = 50\ \mu$m, $\sigma = 0.8$ and $Re_s = 10^6$ and $y_0/a = 1$ (red line in Figure 2) as it passes the sphere. Note the different scales of the vertical axes.

3. The Boundary Layer

In some cases bubbles may collide with the surface of the sphere. Similar phenomena have been noted by Beelen and van Rijsbergen [6]. To prevent these collisions we now include a viscous boundary layer on the surface of the body. A series expansion is used to solve the boundary layer equations at small angle from the stagnation point, using the method described by Crabtree et al [7](PP.421-422). The Newton-Raphson method is then used to solve the boundary layer equations for larger angles. The edge of the boundary layer is defined to be the point at which the tangential velocity is 99% of the external flow

* Corresponding Author: Rhys A. Paul, Rhys.Paul@utas.edu.au

velocity. In all cases, the boundary layer modelled using this method prevents bubbles colliding with the sphere surface. This effect is illustrated in Figure 4, which compares typical microbubble trajectories near the sphere surface in regimes with and without the boundary layer. Five trajectories are shown, representing different starting positions y_0, with initial bubble radius $R_0 = 50\ \mu$m and flow characteristics $\sigma = 0.8$ and $Re_s = 10^6$. The bubbles pass a small way into the boundary layer before moving out to the edge. They are then advected further around the sphere.

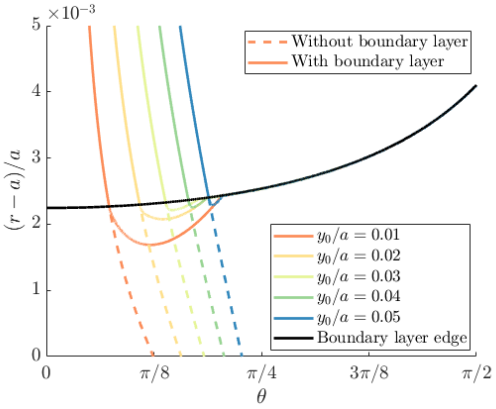

Figure 4. Comparison of bubble trajectories near the sphere with the viscous boundary layer (solid line) and without (dashed line), with varying initial bubble starting heighty_0. Flow parameters are $\sigma = 0.8$ and $Re_s = 10^6$. All bubbles have initial radius $R_0 = 50\ \mu$m and start at $z_0 = -5a$.

4. Conclusions

A numerical method is considered for modelling the dynamics of microbubbles in a potential flow around a sphere. The effect of pressure gradients is found to dominate drag and Kelvin impulse forces and the overall deviation from streamlines is shown to be small. The boundary layer is found to play a critical role in preventing bubbles colliding with the surface.

5. Acknowledgement

The authors wish to acknowledge the support of Australian Defence Science and Technology Group within the framework of the University of Tasmania collaborative work on 2017 US Multidisciplinary University Research Initiative (MURI) entitled: 'Predicting turbulent multi-phase flows with high-fidelity: a physics-based approach'.

References

1. V.E. Johnson and T. Hsieh. The influence of the trajectories of gas nuclei on cavitation inception. In *6th Symposium on Naval Hydrodynamics*, pages 163–179. National Academy Press, 1966.
2. P.A. Brandner, J.A. Venning, and B.W. Pearce. Nucleation effects on cavitation about a sphere (in preparation).
3. Z. Liu, Y. Kuhn de Chizelle, and C.E. Brennen. Cavitation event rates and nuclei distributions. In *ASME Symposium on Cavitation Inception*, FED-Vol. 177, pages 13–23. ASME, 1993.
4. J.P. Franc and J.M. Michel. *Fundamentals of Cavitation*. Springer Science & Business Media, 2005.
5. C.E. Brennen. *Cavitation and Bubble Dynamics*. Cambridge University Press, 1995.
6. S. Beelen and M. van Rijsbergen. Bubble screening in lifting flows and its effect on cavitation inception. *21st Numerical Towing Tank Symposium*, 2018.
7. L.F Crabtree, G.E Gadd, N. Gregory, C.R Illingworth, C.W Jones, D. Küchemann, M.J Lighthill, R.C Pankhurst, L. Rosenhead, L. Sowerby, J.T Stuart, E.J Watson, and G.B Whitham. *Laminar Boundary Layers*. Oxford University Press, 1963.

* Corresponding Author: Rhys A. Paul, Rhys.Paul@utas.edu.au